


# Functional Iron Oxide–Silver Hetero-Nanocomposites: Controlled Synthesis and Antibacterial Activity

VU THI TRANG,<sup>1,2</sup> LE THI TAM,<sup>1</sup> NGUYEN VAN QUY,<sup>3</sup>  
TRAN QUANG HUY,<sup>4</sup> NGUYEN THANH THUY,<sup>4</sup> DOAN QUANG TRI,<sup>1</sup>  
NGUYEN DUY CUONG,<sup>1</sup> PHAM ANH TUAN,<sup>5</sup> HOANG VAN TUAN,<sup>6</sup>  
ANH-TUAN LE,<sup>1,7</sup> and VU NGOC PHAN <sup>1,8</sup>

1.—Advanced Institute for Science and Technology (AIST), Hanoi University of Science and Technology (HUST), No. 1, Dai Co Viet Street, Hai Ba Trung District, Hanoi, Vietnam. 2.—Vietnam Military Medical University, No. 160, Phung Hung Street, Phuc La Ward, Ha Dong District, Hanoi, Vietnam. 3.—International Training Institute for Materials Science (ITIMS), Hanoi University of Science and Technology (HUST), No. 1, Dai Co Viet Street, Hai Ba Trung District, Hanoi, Vietnam. 4.—National Institute of Hygiene and Epidemiology (NIHE), No. 1 Yersin Street, Hai Ba Trung District, Hanoi, Vietnam. 5.—Vietnam Metrology Institute, No. 8, Hoang Quoc Viet Street, Hanoi, Vietnam. 6.—Ministry of Science and Technology of Vietnam, No. 39, Tran Hung Dao Street, Hanoi, Vietnam. 7.—e-mail: tuan.leanh1@hust.edu.vn. 8.—e-mail: phan.vungoc@hust.edu.vn

Iron oxide-silver nanocomposites are of great interest for their antibacterial and antifungal activities. We report a two-step synthesis of functional magnetic hetero-nanocomposites of iron oxide nanoparticles and silver nanoparticles ( $\text{Fe}_3\text{O}_4\text{-Ag}$ ). Iron oxide nanoparticles were prepared first by a coprecipitation method followed by the deposition of silver nanoparticles via a hydrothermal route. The prepared  $\text{Fe}_3\text{O}_4\text{-Ag}$  hetero-nanocomposites were characterized by x-ray diffraction, transmission electron microscopy, high resolution transmission electron microscopy and vibrating sample magnetometry. Their antibacterial activities were investigated by using paper-disk diffusion and direct-drop diffusion methods. The results indicate that the  $\text{Fe}_3\text{O}_4\text{-Ag}$  hetero-nanocomposites exhibit excellent antibacterial activities against two Gram-negative bacterial strains (*Salmonella enteritidis* and *Klebsiella pneumoniae*).

**Key words:**  $\text{Fe}_3\text{O}_4\text{-Ag}$ , hetero-nanocomposites, antibacterial activity, *Salmonella enteritidis*, *Klebsiella pneumoniae*

## INTRODUCTION

In recent years, the synthesis of hybrid nanomaterials based on magnetic nanoparticles (MNPs) and noble metal nanoparticles have attracted tremendous interest due to their unique properties, which make them promising candidates for applications in various fields, such as targeted drug-delivery, cancer treatment, and environmental catalysis.<sup>1–5</sup> For example, the combination of magnetic properties and tunable optical properties allows these hybrid materials to be used as dual probes for

optical-magnetic resonance imaging.<sup>6,7</sup> These materials also exhibit high catalytic activity for various chemical reactions along with magnetically reusable capability.<sup>8–10</sup>

Among noble metal nanoparticles, silver nanocrystals also have great advantages in their antimicrobial properties against various pathogens including bacteria, fungi and viruses.<sup>11–13</sup> There are some well-known mechanisms for the action of silver nanoparticles on bacteria killing: (1) the release of  $\text{Ag}^+$  ions and their strong interaction with thiol groups of L-cysteine residue from proteins, followed by the inactivation of bacterial enzymes, (2) the generation of intracellular reactive oxygen species on the silver surface leading to

oxidative stress, and (3) direct interactions of silver nanoparticles with bacterial cells leading to membrane stress.<sup>14–16</sup> However, due to high surface energy, silver nanocrystals have some drawbacks including low stability and easy aggregation, which can decrease their antibacterial activities. Moreover, the existence of Ag silver or Ag<sup>+</sup> ion residues, which cause toxic effects and cannot be easily removed from water, is also another limitation that needs to be considered.<sup>17</sup> In order to overcome these limitations, silver nanoparticles and MNPs were combined to form hybrid nanomaterials with different structures. For instance, Wei et al. used the thermal decomposition of Fe(CO)<sub>5</sub> on the surface of silver nanoparticles in octadecene to obtain Ag@Fe<sub>2</sub>O<sub>3</sub> yolk-shell nanoparticles, which showed both high capture efficiency of bacteria and potent antibacterial activity against *Escherichia coli* O157:H7 strain.<sup>18</sup> Recently, our group has demonstrated a formation of heterodimer-like Fe<sub>3</sub>O<sub>4</sub>-Ag hybrid nanoparticles through the modified photochemical method.<sup>19</sup> It was shown that the Fe<sub>3</sub>O<sub>4</sub>-Ag hybrid nanoparticles exhibited noticeable antimicrobial properties against *Staphylococcus aureus* bacteria. Moreover, functionalized Ag-MNPs can be used in magnetically assisted surface-enhanced Raman scattering (SERS) biosensors for the detection of *S. aureus* and *Candida* fungal species.<sup>20,21</sup> Wang et al.<sup>20</sup> demonstrated that the aptamer-conjugated Ag-MnFe<sub>2</sub>O<sub>4</sub> NPs is a fast and highly sensitive SERS bioassay for detecting and capturing *S. aureus*, with the limit of detection of 10 cells/mL. Up to now, many different bacterial strains have been studied using iron oxide-silver nanoparticles as antibacterial agents. However, to the best of our knowledge, there are only a few papers on the use of iron oxide-silver hybrid nanomaterials for antibacterial testing against *Klebsiella pneumoniae*<sup>22,23</sup> and no report on *Salmonella enteritidis*. The former, a ubiquitous bacterium in nature, is a common cause of hospital-acquired infections including pneumonia, bloodstream infections, wound infections, urinary tract infections, liver abscesses and meningitis,<sup>24</sup> while the latter is one of the most frequent causes of food poisoning and has become a major health problem in the United States and Europe and also in developing countries.<sup>25–28</sup> Although mainly present in poultry and their eggs, animal meats and milk, *S. enteritidis* has been found in water environments, which can then be a potential source for the transmission of infections.<sup>29–31</sup>

In the present study, we have successfully synthesized iron oxide-silver hetero-nanocomposites and investigated them as antibacterial agents. Iron oxide nanoparticles were prepared first by a simple co-precipitation method and then used as seeds for the formation of silver via a facile hydrothermal synthesis. This synthetic methodology shows some advantages over previously reported methods,

including low costs, simple reactions and large-scale production ability. The prepared Fe<sub>3</sub>O<sub>4</sub>-Ag magnetic nanocomposites were found to exhibit excellent antibacterial activity against two Gram-negative bacteria strains, *S. enteritidis* and *K. pneumoniae*. The results suggest that the Fe<sub>3</sub>O<sub>4</sub>-Ag magnetic nanocomposites can be applied as a reusable antibacterial agent for water disinfection.

## EXPERIMENTAL

### Chemicals

Ferrous chloride tetrahydrate (FeCl<sub>2</sub>·4H<sub>2</sub>O, 98%), ferric chloride hexahydrate (FeCl<sub>3</sub>·6H<sub>2</sub>O, 97%), silver nitrate (AgNO<sub>3</sub>, 99.9%), sodium hydroxide (NaOH), ammonium hydroxide (NH<sub>4</sub>OH, 25%) and poly(vinylpyrrolidone) (PVP) were purchased from Shanghai Chemical Reagent. Other chemicals such as ethanol and deionized water were used. All chemicals were used as received without any purification.

### Preparation of Fe<sub>3</sub>O<sub>4</sub> Nanoparticles

Fe<sub>3</sub>O<sub>4</sub> nanoparticles were prepared by the coprecipitation method described in previous literature with small modifications.<sup>32</sup> Briefly, FeCl<sub>2</sub>·4H<sub>2</sub>O (1 mmol) and FeCl<sub>3</sub>·6H<sub>2</sub>O (2.1 mmol) were dissolved in deionized water in a 1000-mL beaker and stirred at room temperature for 30 min. Then, 80 mL 1 M of sodium hydroxide solution was added dropwise into the above solution at room temperature under vigorous stirring for 30 min. The color of the mixture became black-brown indicating the formation of iron oxide nanoparticles. The black precipitate was collected with an external magnet and the supernatant was decanted. The precipitated Fe<sub>3</sub>O<sub>4</sub> nanoparticles were washed several times with ethanol and deionized water followed by centrifugation (3 min, 3500 rpm).

### Preparation of Fe<sub>3</sub>O<sub>4</sub>-Ag Nanocomposites

In a typical synthesis, 194 mg of as-prepared Fe<sub>3</sub>O<sub>4</sub> nanoparticles and AgNO<sub>3</sub> (0.5 mmol) were mixed in 30 mL deionized water in the presence of 100 mg poly(vinylpyrrolidone) as both reducing and stabilizing agent. This mixture was stirred at room temperature for 1 h. Then, 2.5 mL ammonium hydroxide solution was added dropwise into the mixture under vigorous stirring for 1 h. Next, the mixture was transferred into a Teflon-lined stainless-steel autoclave with a capacity of 70 mL. The sealed vessel was then heated to 200°C and kept at this temperature for 1 h. After the hydrothermal reaction, the autoclave was allowed to cool to room temperature in air. The final products were collected and washed several times in ethanol and water to remove excess surfactant and other materials.

## Characterization Techniques

The morphology and size of the prepared Fe<sub>3</sub>O<sub>4</sub> NPs and Fe<sub>3</sub>O<sub>4</sub>-Ag nanocomposites were characterized by a JEOL JEM 1010 transmission electron microscope (TEM) (80 kV) and a FEI Tecnai G20 high resolution transmission electron microscope (HRTEM) operating at 200 kV. The samples were diluted in ethanol and dropped onto carbon-coated copper grids and then the grids were dried under vacuum at room temperature for 1 h. The crystalline structure of all samples was analyzed by a Bruker D5005 x-ray Diffractometer using graphite-monochromatized CuK $\alpha$  radiation ( $\lambda = 0.154056$  nm) under a voltage of 40 kV and a current of 30 mA. X-ray photoelectron spectroscopy (XPS) measurements were carried out on a Kratos AXIS Ultra-DLD Photoelectron Spectrometer with Al K $\alpha$  monochromatic x-ray source (1486.6 eV). All data were corrected by setting the C 1s peak at 284.5 eV as in Ref. 33. The magnetic hysteresis curves ( $M$ - $H$ ) of the nanocomposites were measured by a vibrating sample magnetometer (VSM) (EZ9, MicroSense) at room temperature.

## Evaluation of Antibacterial Activity

### Bacterial Strains and Culture Medium

Bacterial strains chosen for this study were Gram-negative *S. enteritidis* (*S.E.*) and *K. pneumoniae* (*Kleb.*). These strains were provided by the Department of Virology at the National Institute of Hygiene and Epidemiology (NIHE) in Hanoi.

The growth of cell cultures was executed in a Luria-Bertani medium (1% tryptone, 0.5% yeast extract and 1% NaCl, pH 7). Next, the culture medium containing bacteria was kept in an incubator for 24 h at the temperature 37°C; then, the content of the bacterial culture in it was 10<sup>8</sup> CFU/ml, where the CFU is the colony-forming unit.

### Paper-Disc Diffusion Method

The paper-disc diffusion method was used to evaluate the antibacterial activity of the studied samples against tested bacteria as mentioned previously.<sup>19</sup> Using the spread plate method, nutrient agar plates were inoculated with 100  $\mu$ l of bacterial suspension containing 10<sup>5</sup> CFU. Sterile Whatman No. 1 filter paper discs (diameter 5 mm) loaded with 10  $\mu$ L of samples were placed on the inoculated plates. Control plates were maintained with discs containing distilled water. These plates were incubated at 37°C for 24 h and the zone of inhibition (ZOI) was measured by subtracting the disc diameter from the total inhibition zone diameter.

### Direct-Drop Diffusion Method

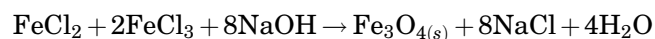
In the next experiment, the direct-drop diffusion method was applied to improve the diffusion ability of Fe<sub>3</sub>O<sub>4</sub>-Ag hetero-nanocomposites in an agar

medium in order to further evaluate the bactericidal activity of the samples. An amount of 5  $\mu$ L of the Fe<sub>3</sub>O<sub>4</sub>-Ag samples at various concentrations of silver (Ag) was directly dropped on the surface of nutrient agar plates inoculated with the studied bacteria suspensions. Control plates were also checked with discs containing distilled water. These plates were incubated at 37°C for 24 h and the antibacterial ability of the samples was observed by optical microscopy.

## RESULTS AND DISCUSSION

### Preparations of Fe<sub>3</sub>O<sub>4</sub> Nanoparticles and Fe<sub>3</sub>O<sub>4</sub>-Ag Hetero-Nanocomposites

Magnetic iron oxide nanoparticles (Fe<sub>3</sub>O<sub>4</sub> NPs) were prepared through the co-precipitation method under alkaline conditions at room temperature. The chemical reaction for the formation of Fe<sub>3</sub>O<sub>4</sub> NPs is as follows:



The particle size and morphology of the as-synthesized products were characterized by TEM. The TEM image in Fig. 1a shows that the Fe<sub>3</sub>O<sub>4</sub> NPs have spherical-like shapes with an average diameter of 20 nm.

The formation of Fe<sub>3</sub>O<sub>4</sub> nanoparticles was also confirmed by x-ray diffraction (XRD) analysis (Fig. 1b). It can be seen that there are eight diffraction peaks at 18.2°, 30.1°, 35.4°, 37.0°, 43.0°, 53.4°, 56.9°, and 62.5°, corresponding to the (111), (220), (311), (222), (400), (422), (511) and (440) planes, respectively, of the face-centered cubic (fcc) structure of magnetite (JCPDS PDF 19-0629). From the XRD pattern, the average crystallite size calculated using the Debye-Scherrer equation is about 19 nm (using the full-width at half-maximum of the Fe<sub>3</sub>O<sub>4</sub> (311) peak), which is consistent with the TEM image.

As described above, the Fe<sub>3</sub>O<sub>4</sub>-Ag nanocomposites were formed by reducing silver nitrate in deionized water in the presence of as-prepared Fe<sub>3</sub>O<sub>4</sub> seed nanoparticles, poly(vinylpyrrolidone) (PVP) and ammonium hydroxide. As shown in Fig. 1c, the TEM image reveals that the obtained Fe<sub>3</sub>O<sub>4</sub>-Ag NPs have a hetero-nanocomposite structure. Because the electron density of Ag NPs is higher than that of Fe<sub>3</sub>O<sub>4</sub> NPs, the Ag NPs appear darker and the Fe<sub>3</sub>O<sub>4</sub> NPs brighter. It can be seen that Ag NPs grew and attached on the surface of the Fe<sub>3</sub>O<sub>4</sub> NPs. Most of the Ag NPs have a particle size between 6 nm and 12 nm. These hetero-nanostructures are somewhat similar to the Fe<sub>3</sub>O<sub>4</sub>-Ag multimer nanoparticles reported by Mao et al.<sup>34</sup> However, in their synthetic process, expensive organic chemicals such as 1-octadecene, oleylamine and trioctylphosphine oxide (TOPO) were required. In contrast, the

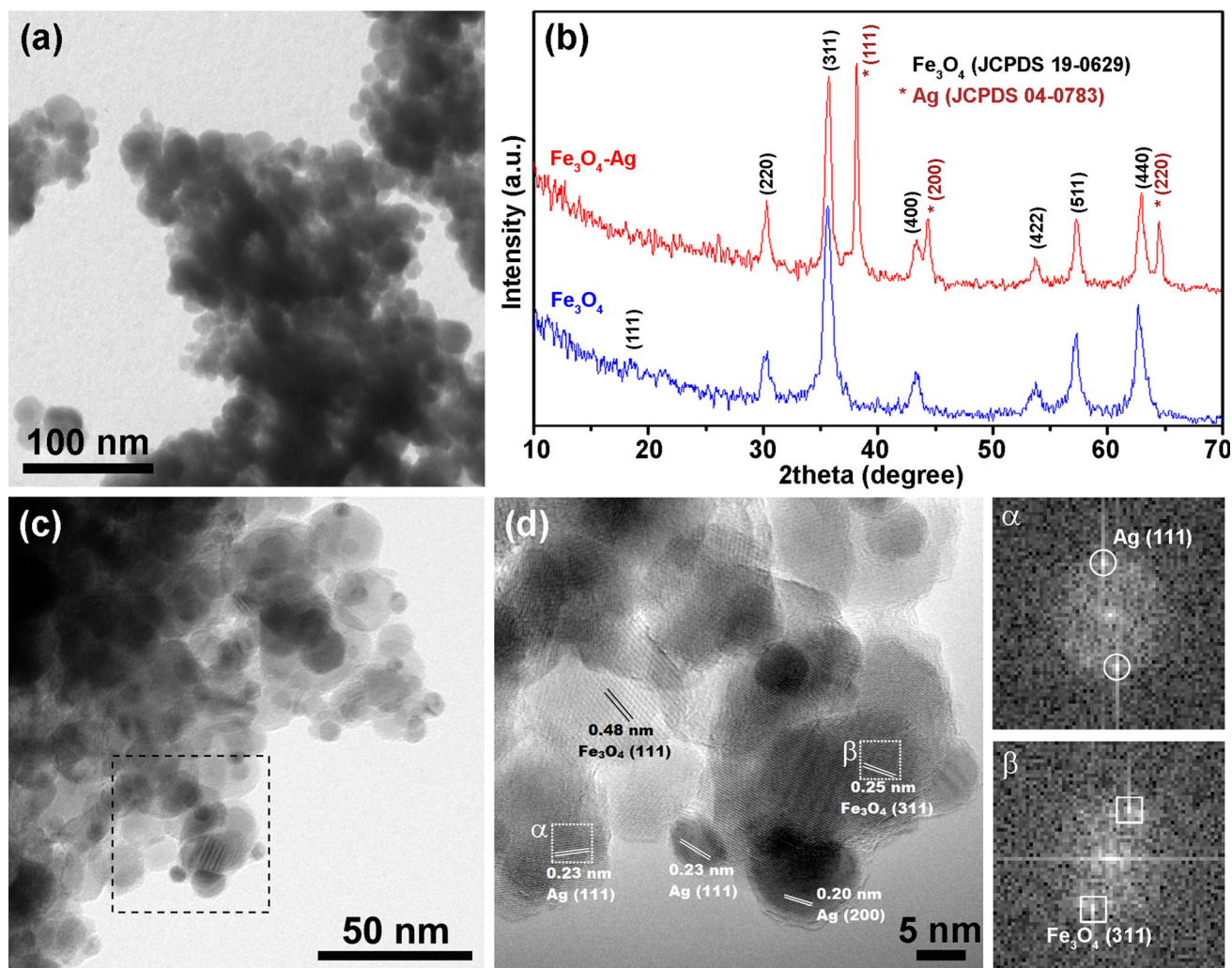


Fig. 1. (a) TEM image of  $\text{Fe}_3\text{O}_4$  nanoparticles; (b) x-ray diffraction patterns of  $\text{Fe}_3\text{O}_4$  NPs and  $\text{Fe}_3\text{O}_4$ -Ag hetero-nanocomposites; (c) TEM and (d) HRTEM images of the  $\text{Fe}_3\text{O}_4$ -Ag hetero-nanocomposites ( $\alpha$ ,  $\beta$ : FFT images of selected areas in the HRTEM image).

procedure outlined above required inexpensive chemicals in aqueous phase.

The structure of the synthesized  $\text{Fe}_3\text{O}_4$ -Ag nanocomposites was also studied by using HRTEM analysis. Figure 1d confirms not only the attachment of Ag NPs on the surface of  $\text{Fe}_3\text{O}_4$  NPs, resulting in the hetero-nanocomposite structure, but also the formation of a single nanocrystalline structure of  $\text{Fe}_3\text{O}_4$ -Ag components. By using Gatan DigitalMicrograph software with the fast Fourier transforms (FFT) option, the lattice fringes of the nanocrystal domain were calculated. The calculated lattice fringes of the two  $\text{Fe}_3\text{O}_4$  domains are 0.25 nm and 0.48 nm, which corresponds to the (311) and (111) planes, respectively. The interfringe spacing of Ag are 0.20 nm and 0.23 nm, close to the interplanar distance of the (200) and (111) planes, respectively. These calculated results are in good agreement with the phases indicated by the XRD pattern in Fig. 1b, where there are three more peaks at  $38.1^\circ$ ,  $44.3^\circ$  and  $64.4^\circ$  corresponding to the

(111), (220) and (311) fcc crystal planes of Ag NPs (JCPDS PDF 04-0783) in comparison to the as-prepared magnetic  $\text{Fe}_3\text{O}_4$  XRD data.

The growth mechanism of Ag NPs on the surface of  $\text{Fe}_3\text{O}_4$  NPs can be proposed as follows: the formation mechanism of the  $\text{Fe}_3\text{O}_4$ -Ag hetero-nanocomposites can be explained by dual roles of PVP. In this reaction, poly(vinylpyrrolidone) is considered to act both as a stabilizing and reducing agent.<sup>35,36</sup> First, the seeds of the as-prepared  $\text{Fe}_3\text{O}_4$  NPs were capped with PVP through the interaction between the carbonyl group of the PVP repeating unit and the Fe atom on the  $\text{Fe}_3\text{O}_4$  NPs.<sup>37</sup> Secondly, a relative stable  $[\text{Ag}(\text{NH}_3)_2]^+$  complex was formed with the addition of an ammonium hydroxide solution to the mixture ( $2\text{NH}_3 + \text{AgNO}_3 \rightarrow [\text{Ag}(\text{NH}_3)_2]^+ + \text{NO}_3^-$ ).<sup>23,38,39</sup> Finally,  $[\text{Ag}(\text{NH}_3)_2]^+$  ions were reduced by the hydroxyl end groups of PVP to form Ag nanoparticles.<sup>40,41</sup> Therefore, PVP performed as a linker between the  $\text{Fe}_3\text{O}_4$  seed NPs and the deposited Ag NPs to obtain the  $\text{Fe}_3\text{O}_4$ -Ag hetero-

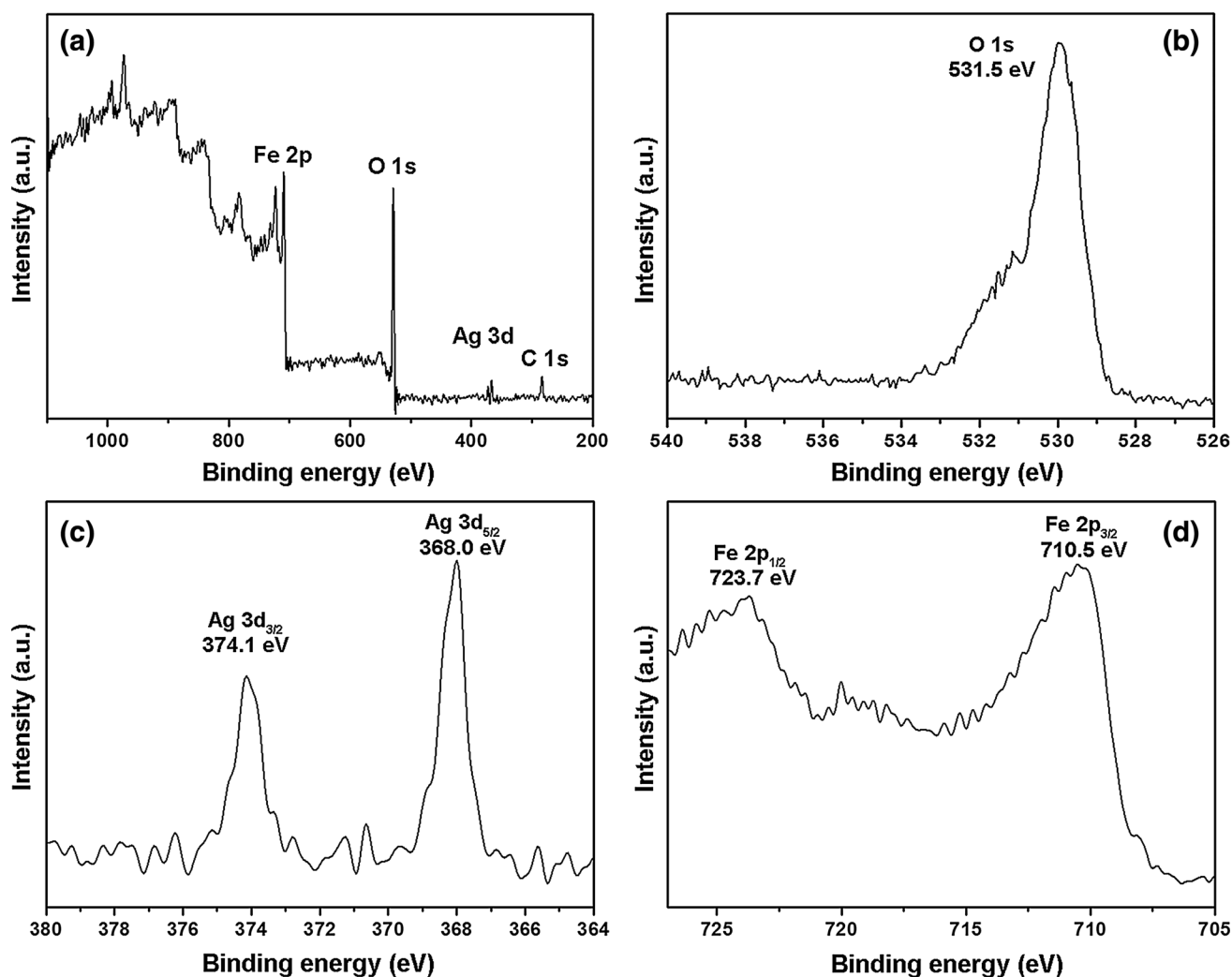


Fig. 2. (a) Full XPS spectrum and (b) O 1s, (c) Ag 3d and (d) Fe 2p XPS spectra of the  $\text{Fe}_3\text{O}_4$ -Ag hetero-nanocomposites.

nanocomposites. Moreover, Gu et al.<sup>42</sup> reported that Fe(II) sites in  $\text{Fe}_3\text{O}_4$  NPs could act as the catalytic center for the reduction of  $\text{Ag}^+$  and the nucleation of Ag NPs.

In order to verify the chemical composition and oxidation states of the obtained  $\text{Fe}_3\text{O}_4$ -Ag hetero-nanocomposites, XPS measurements were carried out. A wide-scan XPS survey and high-resolution XPS patterns for Fe 3p, Ag 3d and O 1s are shown in Fig. 2. Figure 2b shows the high-resolution XPS spectrum of O 1s, and the peak at about 531.5 eV corresponds to the hydroxyl group (O-H),<sup>43</sup> which confirms the presence of PVP in the nanocomposites.<sup>44</sup> The photoelectron spectrum for the Ag 3d region is shown in Fig. 2c, where the two peaks observed at about 368.0 eV and 374.1 eV are attributed to Ag 3d<sub>5/2</sub> and Ag 3d<sub>3/2</sub>, respectively. This result is in good agreement with the standard XPS data for bulk silver.<sup>33</sup> The spin-orbit splitting of the 3d doublet is 6.1 eV, which also indicates the formation of metallic silver nanoparticles ( $\text{Ag}^0$ ) on the iron oxide nanoparticles.<sup>45</sup> As indicated in

Fig. 2d, the double Fe 2p peaks were located at binding energies of 723.7 eV (Fe 2p<sub>1/2</sub>) and 710.5 eV (Fe 2p<sub>3/2</sub>), which are consistent with  $\text{Fe}_3\text{O}_4$  characteristics.<sup>46</sup>

The magnetic properties of the pristine  $\text{Fe}_3\text{O}_4$  NPs and the  $\text{Fe}_3\text{O}_4$ -Ag hetero-nanocomposites with different Ag contents were monitored by measuring the hysteresis loops in a VSM magnetometer at room temperature (300 K) by cycling the field between  $-20,000$  and  $+20,000$  Oe, as illustrated in Fig. 3. All the samples were found to exhibit ferromagnetic behavior at 300 K. In particular, the saturation magnetization ( $M_s$ ) of  $\text{Fe}_3\text{O}_4$  NPs is 53.3 emu/g, the remanent magnetization ( $M_r$ ) is 0.54 emu/g and the coercive force ( $H_c$ ) is 3.89 Oe. It can be seen that the growth of Ag NPs on the surface of the  $\text{Fe}_3\text{O}_4$  seed NPs had a small effect on the magnetic properties of the materials. The  $M_s$  value of the  $\text{Fe}_3\text{O}_4$ -Ag hetero-nanocomposites prepared with 0.5 mmol  $\text{AgNO}_3$  is 37.87 emu/g. In order to evaluate the effect of silver content in the nanocomposites on their magnetic properties, some

$\text{Fe}_3\text{O}_4$ -Ag nanocomposite samples were synthesized with higher  $\text{AgNO}_3$  concentrations. When the  $\text{Ag}^+$  concentration was increased to 1.5 mmol and 2.5 mmol, the saturation magnetizations of the  $\text{Fe}_3\text{O}_4$ -Ag hetero-nanocomposites varied slightly from 37.21 emu/g to 34.5 emu/g, respectively. It is obvious that the formation of Ag NPs resulted in the decrease in magnitude of the nanocomposites  $M_s$  which are due to the weight contribution of the non-magnetic phase. The inset in Fig. 3 shows that the hetero-nanocomposites can be separated from the solution by using an external magnet. This result indicates that the prepared  $\text{Fe}_3\text{O}_4$ -Ag hybrids are useful for magnetically assisted separation applications.

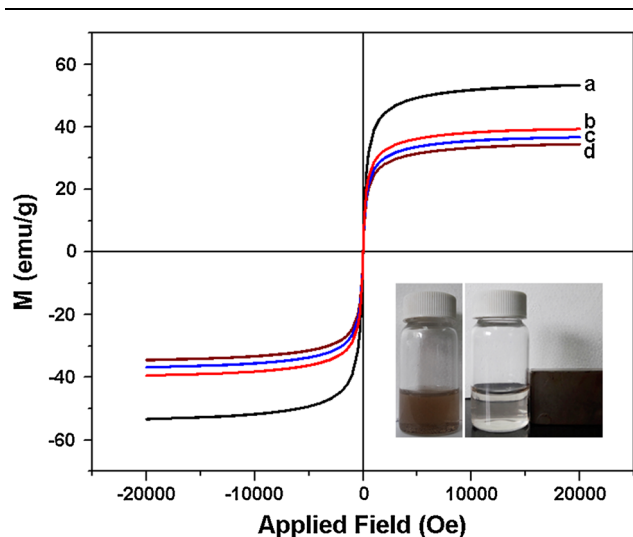


Fig. 3. Room-temperature magnetization curves ( $M$ - $H$ ) of (a)  $\text{Fe}_3\text{O}_4$  NPs and (b-d)  $\text{Fe}_3\text{O}_4$ -Ag hetero-nanocomposites with different  $\text{Ag}^+$  concentrations of (b) 0.5 mmol, (c) 1.5 mmol and (d) 2.5 mmol (Inset: nanocomposite solutions before and after magnetic separation by an external magnet).

Fig. 5. (a, b) Agar plates and (c-j) optical microscopic images of antibacterial tests against (left) *Salmonella enteritidis* and (right) *Klebsiella pneumoniae* bacteria by the direct-drop diffusion method with (c, d) the pristine  $\text{Fe}_3\text{O}_4$  and (e-j) the  $\text{Fe}_3\text{O}_4$ -Ag hetero-nanocomposites at different concentrations: (e, f) 386 ppm, (g, h) 771 ppm and (i, j) 1542 ppm.

### Antibacterial Activity $\text{Fe}_3\text{O}_4$ -Ag Hetero-Nanocomposites

The antimicrobial properties of  $\text{Fe}_3\text{O}_4$ -Ag hetero-nanocomposites were studied on two bacteria strains by employing the standard disk diffusion assay on Luria-Bertani medium. Two Gram-negative bacteria, *S.E.* and *Kleb.*, were chosen as models for antibacterial analyses. These infectious bacteria strains are the main reasons for outbreaks of food-borne and nosocomial infections causing a serious threat to community and human health.

The disk diffusion assay was performed by placing a 5-mm filter paper treated with 10  $\mu\text{L}$  of the  $\text{Fe}_3\text{O}_4$  NPs or the  $\text{Fe}_3\text{O}_4$ -Ag hetero-nanocomposites onto an agar plate seeded with approximate  $10^5$  CFU of *S.E.* and *Kleb.* bacteria. Then, these plates were incubated at 37°C for 24 h. The ZOI was determined by measuring the diameter of inhibition zones. Additionally, the control cultures (with DI water only in the absence of any samples) were used as control samples for comparison.

In our tests, five samples were investigated with different concentrations of the  $\text{Fe}_3\text{O}_4$ -Ag hetero-nanocomposites in the range from 96 ppm to 1542 ppm. Figure 4 shows photographs of two agar plates for antimicrobial tests against (a) *S.E.* and (b) *Kleb.* bacteria. It can be seen that the  $\text{Fe}_3\text{O}_4$ -Ag hetero-nanocomposites have antibacterial activity against both bacteria and that the inhibition zone diameter increases with an increase of the silver concentration. In Fig. 4a, no inhibition effect was found in the control sample and at low

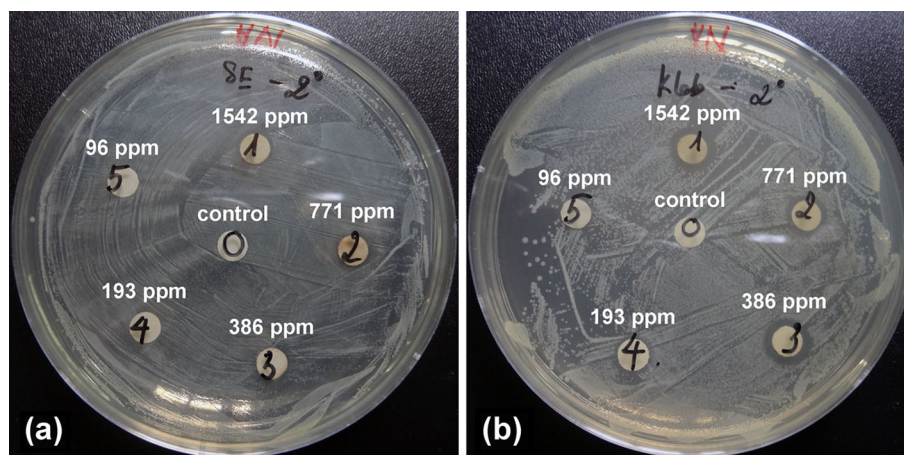
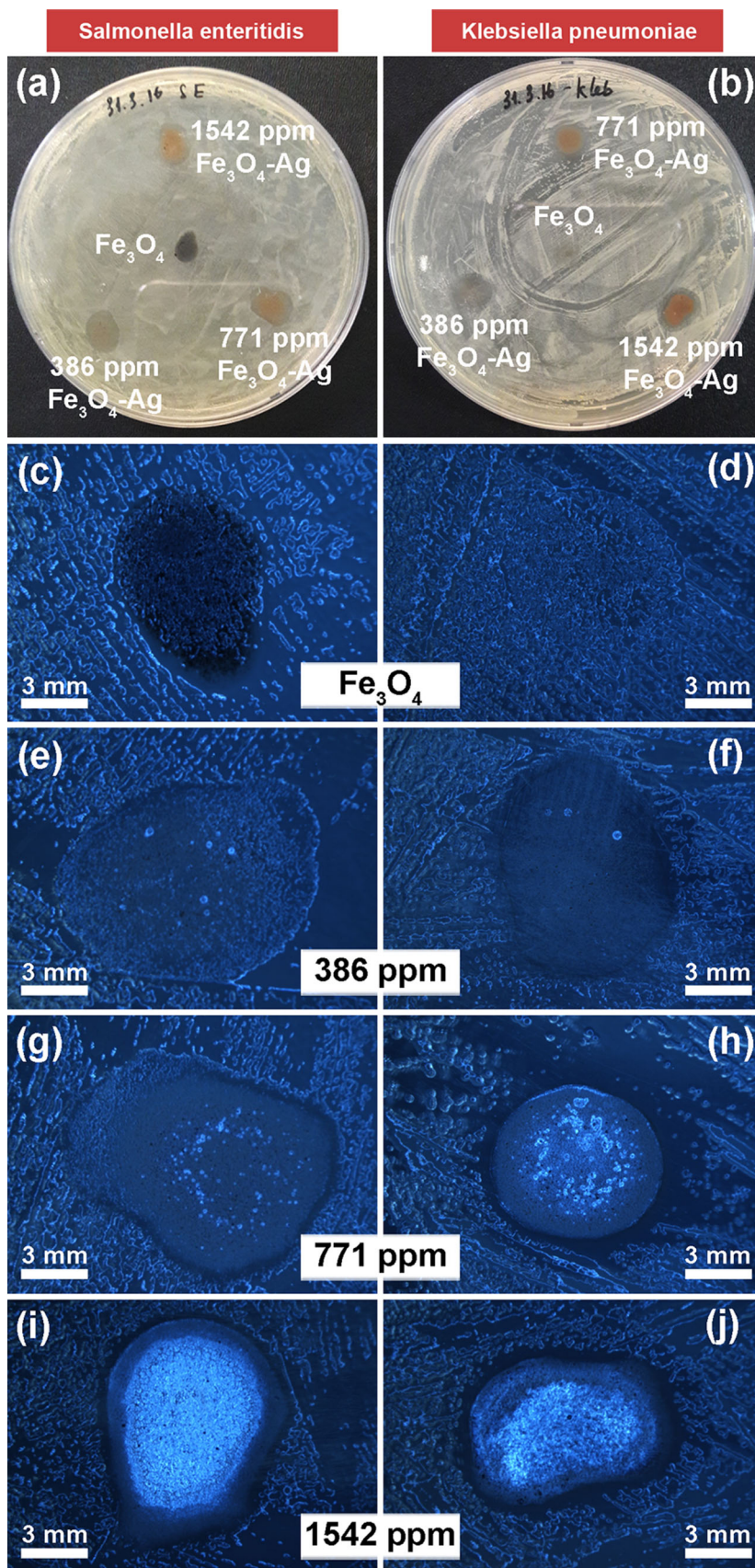


Fig. 4. Antibacterial tests against (a) *Salmonella enteritidis* and (b) *Klebsiella pneumoniae* after the incubation at 37°C for 24 h with different concentrations of prepared  $\text{Fe}_3\text{O}_4$ -Ag hetero-nanocomposites by the paper-disc diffusion method.



concentrations of 96 ppm and 193 ppm, whereas the ZOI could be observed at higher concentrations. The larger ZOI observed in Fig. 4b indicates that the Fe<sub>3</sub>O<sub>4</sub>-Ag hetero-nanocomposites have higher antibacterial activity (higher diameter of inhibition zone) against *Kleb.* than *S.E.*, even at a low concentration of 193 ppm.

Previous studies<sup>13,19,23</sup> have shown that the antibacterial mechanism of Ag-based nanomaterials was strongly related to the direct contacts of nanomaterials with bacterial cells. The increase of interactions between them can improve their bactericidal activity. To further demonstrate an effective means of interactions between nanocomposites and bacterial cells, we employed the direct-drop diffusion method to study the antibacterial activities of the nanocomposite materials. In this method, solutions of the Fe<sub>3</sub>O<sub>4</sub>-Ag hetero-nanocomposites with different concentrations were directly dropped onto the agar plates treated with approximately 10<sup>5</sup> CFU of both *S.E.* and *Kleb.* bacteria, followed by the incubation at 37°C for 24 h. The antimicrobial effect of pristine Fe<sub>3</sub>O<sub>4</sub> NPs on these bacteria was also tested for comparison.

Figure 5a and b are images of agar plates containing *S.E.* and *Kleb.* respectively, after treatment using the pristine Fe<sub>3</sub>O<sub>4</sub> NPs and the Fe<sub>3</sub>O<sub>4</sub>-Ag hetero-nanocomposites by direct-drop diffusion assay. It can be observed that Fe<sub>3</sub>O<sub>4</sub> NPs had no effect on the growth of either bacteria, whereas the inhibition zones were found in the case of Fe<sub>3</sub>O<sub>4</sub>-Ag nanocomposites (Fig. 5c and d). For more detail, an optical microscope was used to take photographs at the sites where the Fe<sub>3</sub>O<sub>4</sub> and Fe<sub>3</sub>O<sub>4</sub>-Ag solutions were dropped (Fig. 5c–j). Figure 5c and d shows that the bacteria grew drastically in the presence of just Fe<sub>3</sub>O<sub>4</sub> NPs. However, if the Fe<sub>3</sub>O<sub>4</sub>-Ag hetero-nanocomposites solution was dropped onto bacteria-treated plates, the growth of the bacteria decreased. Figure 5e shows that the *S.E.* bacteria could grow up to a concentration of 386 ppm of Fe<sub>3</sub>O<sub>4</sub>-Ag. Even at a two-fold content of 771 ppm (Fig. 5g), *S.E.* bacteria were still alive although an inhibition zone could be observed. When increasing the silver content to a higher concentration (1542 ppm), the bacteria growth was reduced and the ZOI was clearly found (Fig. 5i).

With the same concentrations, the Fe<sub>3</sub>O<sub>4</sub>-Ag hetero-nanocomposites exhibited higher inhibition effects against *Kleb.* bacteria in comparison with *S.E.* bacteria as seen in Fig. 5f, i, and j. At the concentration of 386 ppm, most bacteria were prohibited and a ZOI can be observed (Fig. 5f). Larger inhibition zones appeared when the concentration was raised to higher values, showing a noticeable inhibition effect of the Fe<sub>3</sub>O<sub>4</sub>-Ag hetero-nanocomposites against *Kleb.* bacteria (Fig. 5h, i, and j). These results indicate that the prepared magnetic Fe<sub>3</sub>O<sub>4</sub>-Ag hetero-nanocomposites have excellent antimicrobial activities against these bacteria.

## CONCLUSIONS

In summary, we report a simple and effective synthesis of magnetic Fe<sub>3</sub>O<sub>4</sub>-Ag hetero-nanocomposites. By using a facile hydrothermal technique with the presence of poly(vinylpyrrolidone) as both surfactant and reducing agent, silver nanoparticles were deposited on the surface of Fe<sub>3</sub>O<sub>4</sub> seed nanoparticles to form the hybrid nanostructures. The resulting iron oxide–silver hetero-nanocomposites exhibited high antibacterial activities against *S. enteritidis* and especially *K. pneumoniae* bacteria. We believe that the hetero-nanocomposites can be used not only for recyclable antimicrobial application but also for other applications such as magnetic separation and bio-sensors.

## ACKNOWLEDGEMENTS

This research was funded by Vietnam National Foundation for Science and Technology Development (NAFOSTED) under grant number 103.02-2013.35. The authors would like to acknowledge the supports for HRTEM measurements from Electron Microscopy Center, School of Materials, University of Manchester, UK. Also, the technical supports for biological measurements at National Institute of Hygiene and Epidemiology (NIHE) are acknowledged. The authors thank Advanced Institute for Science and Technology (AIST), Hanoi University of Science and Technology for the usage of their VSM instrument.

## REFERENCES

1. R. Costi, A.E. Saunders, and U. Banin, *Angew. Chem. Int. Ed.* 49, 4878 (2010).
2. K.C.-F. Leung and S. Xuan, *Chem. Rec.* 16, 458 (2016).
3. N.C. Bigall, W.J. Parak, and D. Dorfs, *Nano Today* 7, 282 (2012).
4. G. Li and Z. Tang, *Nanoscale* 6, 3995 (2014).
5. H. Woo and K.H. Park, *Catal. Today* 278, 209 (2016).
6. S. Narayanan, B.N. Sathy, U. Mony, M. Koyakutty, S.V. Nair, and D. Menon, *ACS Appl. Mater. Interfaces* 4, 251 (2011).
7. C. Xu, J. Xie, D. Ho, C. Wang, N. Kohler, E.G. Walsh, J.R. Morgan, Y.E. Chin, and S. Sun, *Angew. Chem. Int. Ed.* 47, 173 (2008).
8. J. Chung, J. Kim, Y. Jang, S. Byun, T. Hyeon, and B.M. Kim, *Tetrahedron Lett.* 54, 5192 (2013).
9. S. Byun, Y. Song, and B.M. Kim, *ACS Appl. Mater. Interfaces* 8, 14637 (2016).
10. M. Zhu, C. Wang, D. Meng, and G. Diao, *J. Mater. Chem. A* 1, 2118 (2013).
11. M.K. Rai, S.D. Deshmukh, A.P. Ingle, and A.K. Gade, *J. Appl. Microbiol.* 112, 841 (2012).
12. S. Eckhardt, P.S. Brunetto, J. Gagnon, M. Priebe, B. Giese, and K.M. Fromm, *Chem. Rev.* 113, 4708 (2013).
13. Q.H. Tran, V.Q. Nguyen, and A.-T. Le, *Adv. Nat. Sci. Nanosci. Nanotechnol.* 4, 033001 (2013).
14. H.-J. Park, J.Y. Kim, J. Kim, J.-H. Lee, J.-S. Hahn, M.B. Gu, and J. Yoon, *Water Res.* 43, 1027 (2009).
15. G.A. Sotiriou and S.E. Pratsinis, *Environ. Sci. Technol.* 44, 5649 (2010).
16. C. Marambio-Jones and E.M.V. Hoek, *J. Nanoparticle Res.* 12, 1531 (2010).
17. C. Levard, E.M. Hotze, G.V. Lowry, and G.E. Brown Jr, *Environ. Sci. Technol.* 46, 6900 (2012).
18. Z. Wei, Z. Zhou, M. Yang, C. Lin, Z. Zhao, D. Huang, Z. Chen, and J. Gao, *J. Mater. Chem.* 21, 16344 (2011).



19. L.M. Tung, N.X. Cong, L.T. Huy, N.T. Lan, V.N. Phan, N.Q. Hoa, L.K. Vinh, N.V. Thinh, L.T. Tai, and K. Mølhave, *J. Nanosci. Nanotechnol.* **16**, 5902 (2016).
20. J. Wang, X. Wu, C. Wang, N. Shao, P. Dong, R. Xiao, and S. Wang, *ACS Appl. Mater. Interfaces* **7**, 20919 (2015).
21. T. Donnelly, W.E. Smith, K. Faulds, and D. Graham, *Chem. Commun.* **50**, 12907 (2014).
22. P. Dallas, J. Tucek, D. Jancik, M. Kolar, A. Panacek, and R. Zboril, *Adv. Funct. Mater.* **20**, 2347 (2010).
23. R. Prucek, J. Tuček, M. Kilianová, A. Panáček, L. Kvítek, J. Filip, M. Kolář, K. Tománková, and R. Zboril, *Biomaterials* **32**, 4704 (2011).
24. M.K. Paczosa and J. Mecsas, *Microbiol. Mol. Biol. Rev.* **80**, 629 (2016).
25. R. Putturu, T. Eevuri, B. Ch, and K. Nelapati, *Int. J. Pharm. Biol. Sci.* **5**, 86 (2015).
26. W.M. Linam and M.A. Gerber, *Pediatr. Infect. Dis. J.* **26**, 747 (2007).
27. C.R. Lane, S. LeBaigue, O.B. Esan, A.A. Awofisyo, N.L. Adams, I.S. Fisher, K.A. Grant, T.M. Peters, L. Larkin, and R.H. Davies, *Emerg. Infect. Dis.* **20**, 1097 (2014).
28. T.H. Vo, N.H. Le, T.T.D. Cao, J.P. Nuorti, and N.N.T. Minh, *Int. J. Infect. Dis.* **26**, 128 (2014).
29. E.J. Threlfall, *FEMS Microbiol. Rev.* **26**, 141 (2002).
30. E. Landeras, M.A. González-Hevia, and M.C. Mendoza, *Int. J. Food Microbiol.* **43**, 81 (1998).
31. I. Graeber, M.A. Montenegro, C. Bunge, U. Boettcher, H. Tobias, E.A. Heinemeyer, and R. Helmuth, *Eur. J. Epidemiol.* **11**, 325 (1995).
32. Y.S. Kang, S. Risbud, J.F. Rabolt, and P. Stroeve, *Chem. Mater.* **8**, 2209 (1996).
33. J.F. Moulder, W.F. Stickle, P.E. Sobol, and K.D. Bomben, *Handbook of X-Ray Photoelectron Spectroscopy* (Eden Prairie: Perkin-Elmer, 1992).
34. Y. Mao, P. Yi, Z. Deng, and J. Ge, *CrystEngComm* **15**, 3575 (2013).
35. C.E. Hoppe, M. Lazzari, I. Pardiñas-Blanco, and M.A. López-Quintela, *Langmuir* **22**, 7027 (2006).
36. K.M. Koczkur, S. Mourdikoudis, L. Polavarapu, and S.E. Skrabalak, *Dalton Trans.* **44**, 17883 (2015).
37. Y. Zhang, J.-Y. Liu, S. Ma, Y.-J. Zhang, X. Zhao, X.-D. Zhang, and Z.-D. Zhang, *J. Mater. Sci. Mater. Med.* **21**, 1205 (2010).
38. A. Amarjargal, L.D. Tijing, I.-T. Im, and C.S. Kim, *Chem. Eng. J.* **226**, 243 (2013).
39. V.G. Pol, D.N. Srivastava, O. Palchik, V. Palchik, M.A. Slifkin, A.M. Weiss, and A. Gedanken, *Langmuir* **18**, 3352 (2002).
40. I. Washio, Y. Xiong, Y. Yin, and Y. Xia, *Adv. Mater.* **18**, 1745 (2006).
41. K. Zhao, C. Wu, Z. Deng, Y. Guo, and B. Peng, *RSC Adv.* **5**, 52726 (2015).
42. H. Gu, Z. Yang, J. Gao, C. Chang, and B. Xu, *J. Am. Chem. Soc.* **127**, 34 (2005).
43. J. Mu, B. Chen, Z. Guo, M. Zhang, Z. Zhang, P. Zhang, C. Shao, and Y. Liu, *Nanoscale* **3**, 5034 (2011).
44. J. Ma, K. Wang, and M. Zhan, *ACS Appl. Mater. Interfaces* **7**, 16027 (2015).
45. X. Liu, R. Jin, D. Chen, L. Chen, S. Xing, H. Xing, Y. Xing, and Z. Su, *J. Mater. Chem. A* **3**, 4307 (2015).
46. T. Yamashita and P. Hayes, *Appl. Surf. Sci.* **254**, 2441 (2008).